Present status and future prospects of the application of liquid metals for plasma-facing components in magnetic fusion devices

TOFE-2014
Nov. 9-14th
Anaheim, USA

Yoshi Hirooka（NIFS), G. Mazzitelli (ENEA), S. Mirnov (TRINITY), M. Ono (PPPL), M. Shimada (JAEA), F. L. Tabares (CIEMAT)

Table of contents

"Chicken-Egg" Boundary control effect ①
Reduced edge density => improved core confinement

Supershots in TFTR

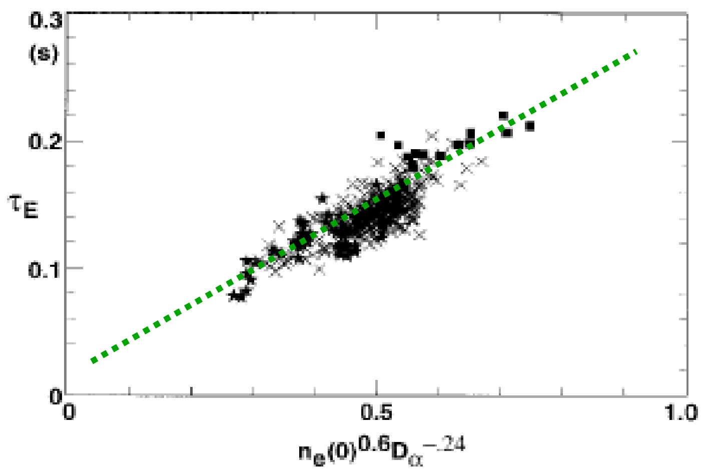

After J.D.Strachan, Nucl. Fusion 39(1999)1093.

From the TFTR supershot database:

$$\tau_E \propto n_e^{0.6} / D_\alpha^{2.4}$$

where

$$\tau_E = \frac{W}{Q_{ext} + Q_\alpha}, \quad W = \int 3(n_i + n_e) T d^3x = 3\overline{nTV})$$

Super dense core in LHD

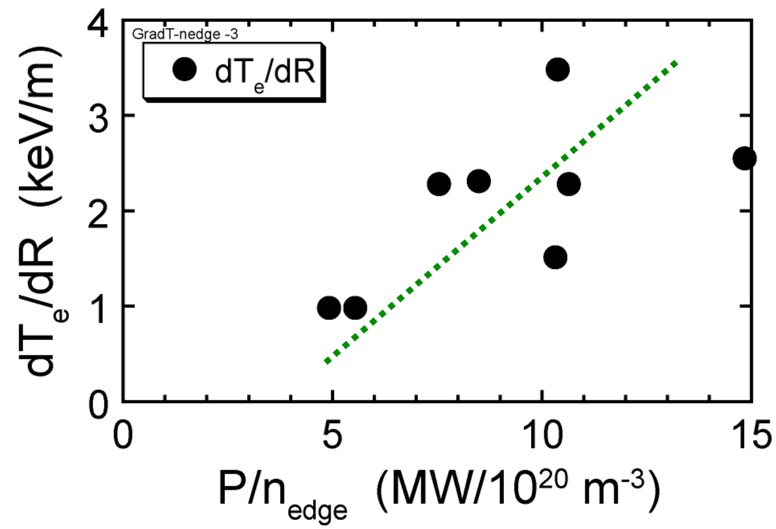

After N. Ohyabu et al., PRL97(2006)055002.

From the LHD superdense-core plasma exps.:

$$\chi = \frac{1}{2}(\chi_e + \chi_i) = -\frac{1}{2}\frac{q_e + q_i}{n_e (dT/dR)}$$

(*after G. Becker, Nucl. Fusion* 44(2004)*L*26)

"Chicken-Egg" Boundary control effect ②
Improved core confinement => reduced edge density

L-to-H mode transition with ETB in ASDEX

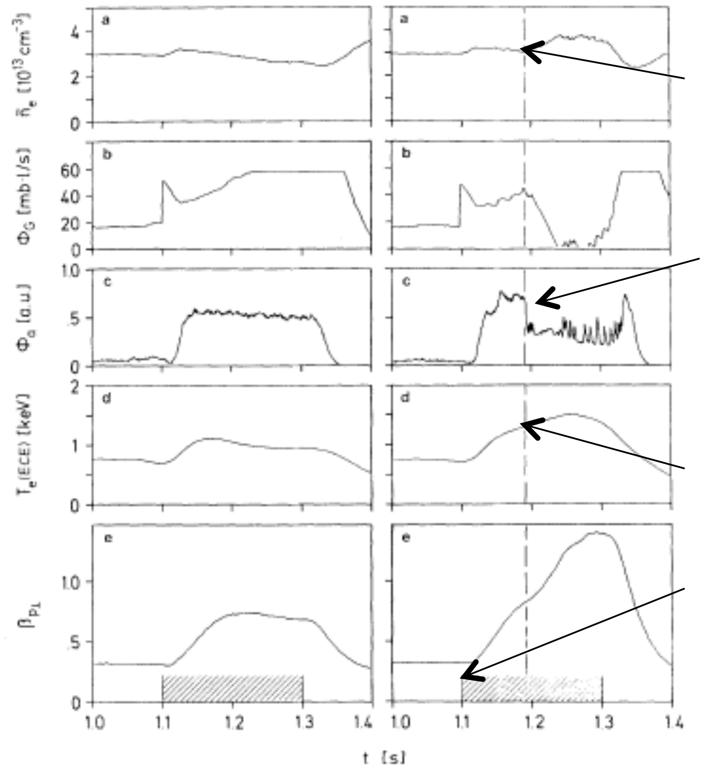

Density increase

Edge density decrease

Temperature increase

NBI-heating start

FIG. 1. Time dependence of various plasma parameters of L-type (left column) and H-type (right column) discharges: (a) line averaged density $\bar{n}_e$, (b) external gas flux φ_G, (c) atom flux φ_a ($E = 273$ eV) reflected from the divertor neutralizer plate, (d) central electron temperature, and (e) beta poloidal. The neutral injection phase is indicated by the hatched time interval. The dashed vertical line indicates the transition from the L to the H regime (see text).

After F. Wagner et al. PRL 49(1982)1408

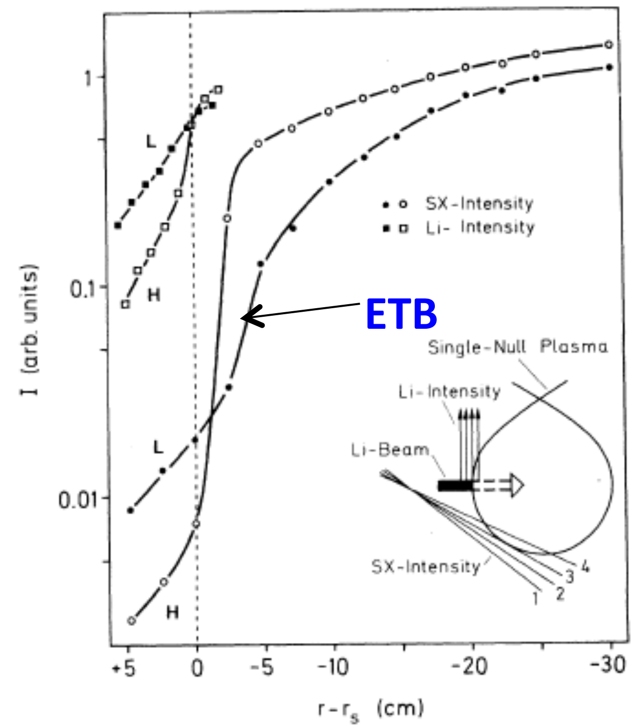

FIG. 2. Radial profiles of the SX (2-μm Be filter) and Li-beam intensities in the L phase prior to the H transition and shortly afterwards (SX, $\Delta t = 20$ ms; Li, $\Delta t = 55$ ms). $I_p = 375$ kA, $B_T = 2.2$ T, $\bar{n}_e = 3.3\times10^{13}$ cm^{-3}, $P_{NI} = 0.8$ MW. The inset depicts the observation geometry.

Edge transport barrier

$$D_\perp = -\frac{\Gamma_{out}}{(dn/dr)}$$

After F. Wagner et al. PRL 53(1984)1408

Technical issues with present-day PFCs

ITER-divertor

- **W-armor + <u>Cu alloy</u> heat sink**

  Divertor heat flux : 10~20MW/m²

  Plasma current~15MA

  Heating power～100MW

  PFC power width: λ_q= ~ 5㎜

Eich NF2013

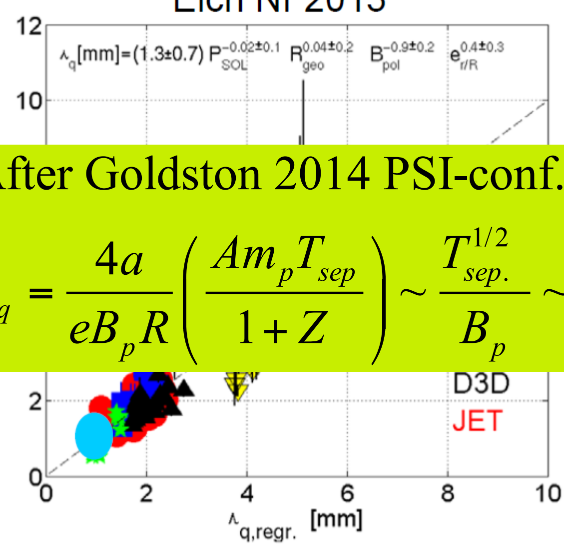

After Goldston 2014 PSI-conf.:

$$\lambda_q = \frac{4a}{eB_pR}\left(\frac{Am_pT_{sep}}{1+Z}\right) \sim \frac{T_{sep.}^{1/2}}{B_p} \sim \frac{1}{I_p}$$

After Loarte presented at 2014 PSI-conf.

DEMO-divertor

- **W-armor + <u>F82H</u> heat sink**

  Max. heat flux : ～8MW/m²

  Plasma current~20-30MA

  Heating power~500MW

  PFC power width: λ_q= ~ 1㎜

- **Need for an innovative PFC ! !**

  Possible metals and/or alloys:

  Ga（T_m=29.8℃, Z=31）

  Li(T_m=186℃, Z=3)

  Sn（T_m=231℃, Z=50）

  $Li_{17}Pb_{83}$（T_m=235℃, Z=69*）

DBTT(~400d°C) cracking on tungsten-PFC

Thermal cycle cracking

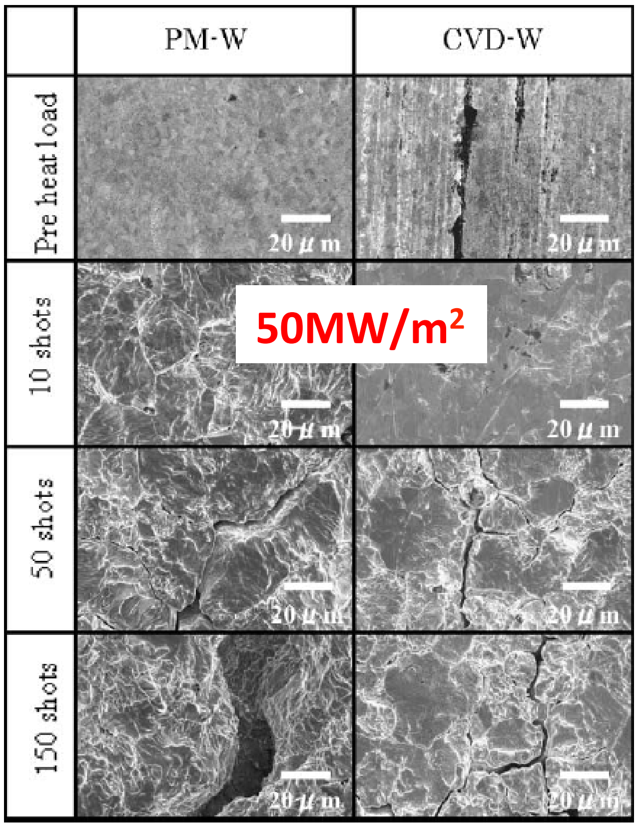

Fig. 3. SEM micrographs of the surface of CVD-W/Mo (surface temperature: 1250–1300 °C) and PM-W (surface temperature: 1280–1380 °C) after heat load tests at a heat flux of 50 MW/m^2, 30 s.

Hydrogen-implantation cracking

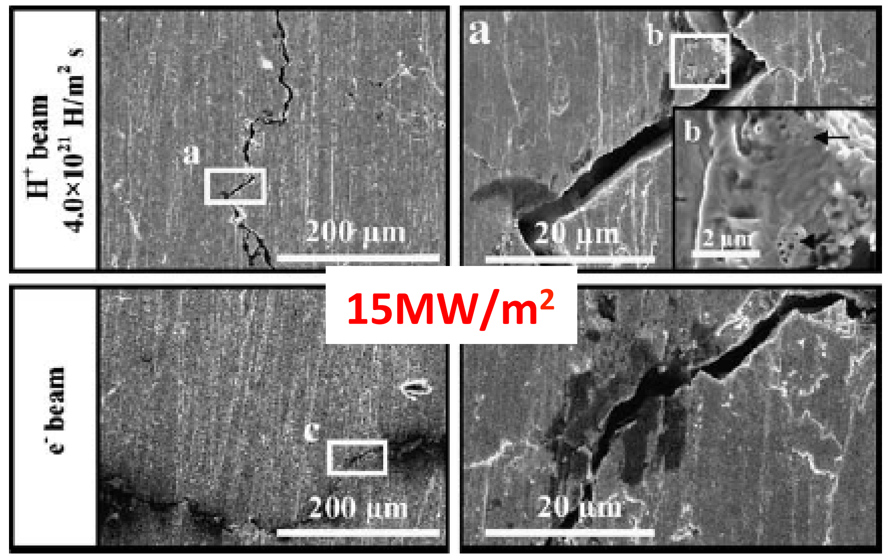

Fig. 4. Surface morphology of the samples after 110 shots with a peak temperature of 1600 °C. Small pores are observed at the coating surface (b) after hydrogen beam irradiation.

Potential issues on liquid metal PFC concepts

After A. Ying (UCLA)

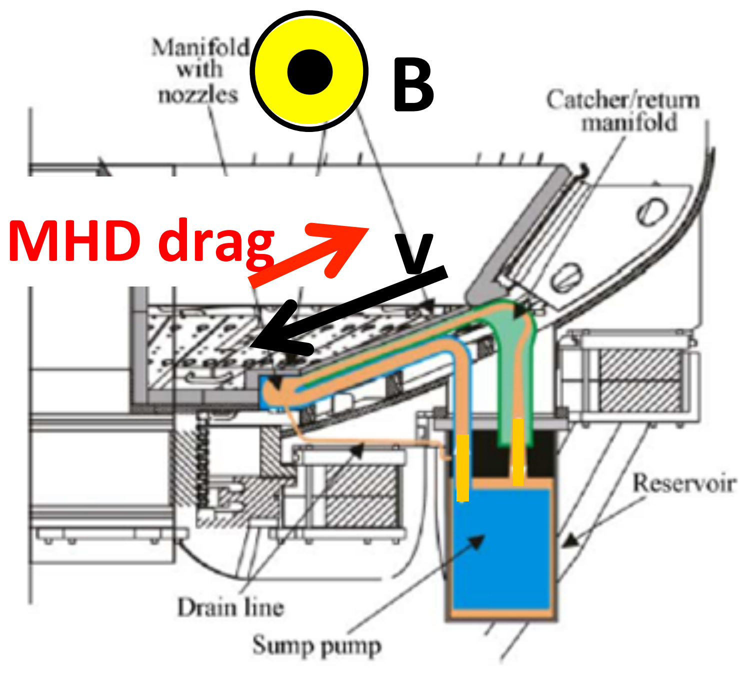

After M. Ono (PPPL NSTX-U)

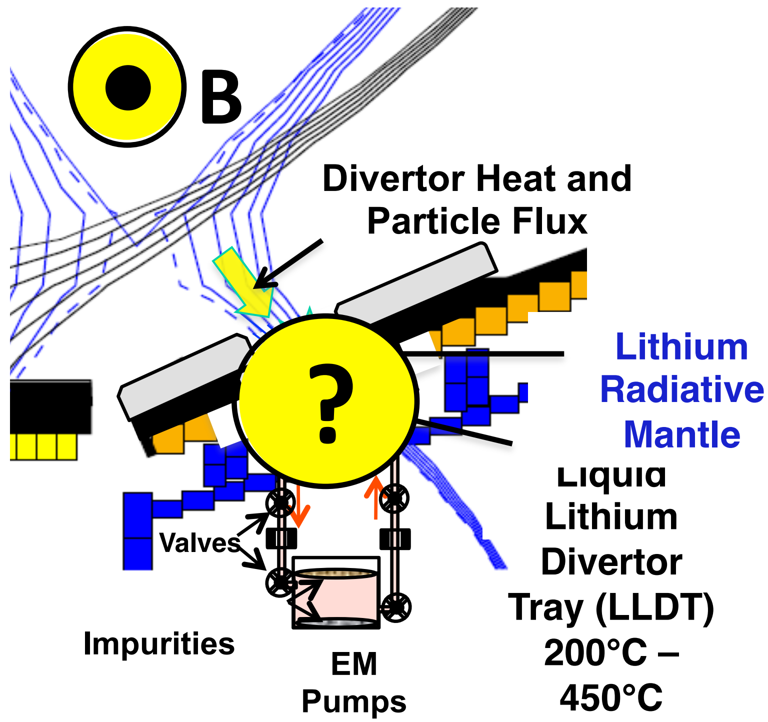

CPS-limiter(s) in T11, FTU, TJ-II, etc.

Li-coatings have induced H-mode in TJ-II

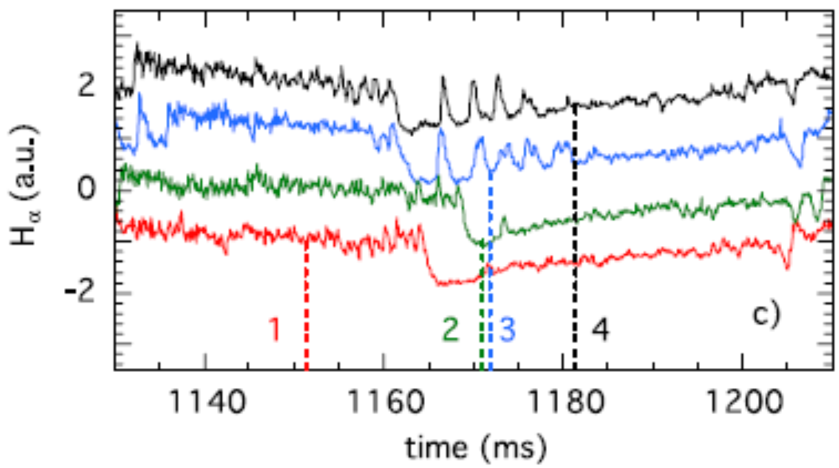

Figure 9. Time evolution of line density (*a*), diamagnetic energy (*b*) and Hα signal (*c*) in four similar discharges during the L–H transition. In (*c*), the vertical lines and the numbers, from 1 to 4, correspond to the time instants of the Thomson scattering diagnostic measurement in each discharge (the respective density profiles are shown in figure 10).

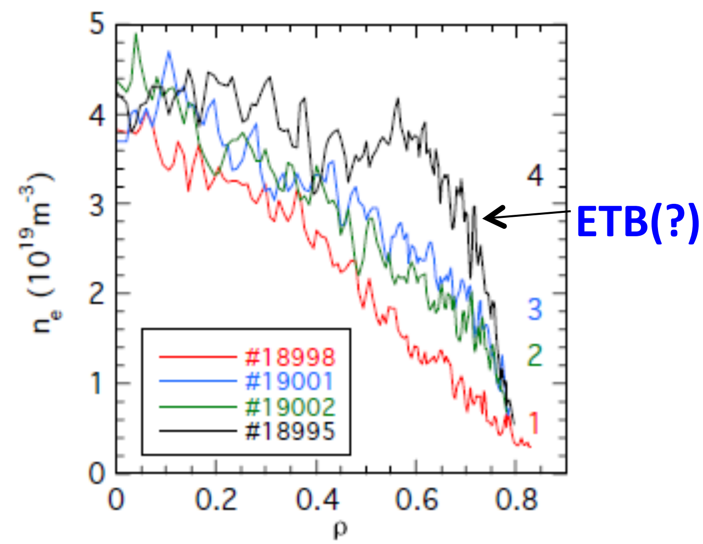

Figure 10. Evolution of the electron density profile during the L–H transition. The profiles are measured using the Thomson scattering diagnostic in the discharges and time instants shown in figure 9.

After Sanchez et al. Nucl. Fusion4(2009)104018.

Lithium emission-collection "loop" in T11

After Mirnov, paper presented at the IAEA-FEC 2014

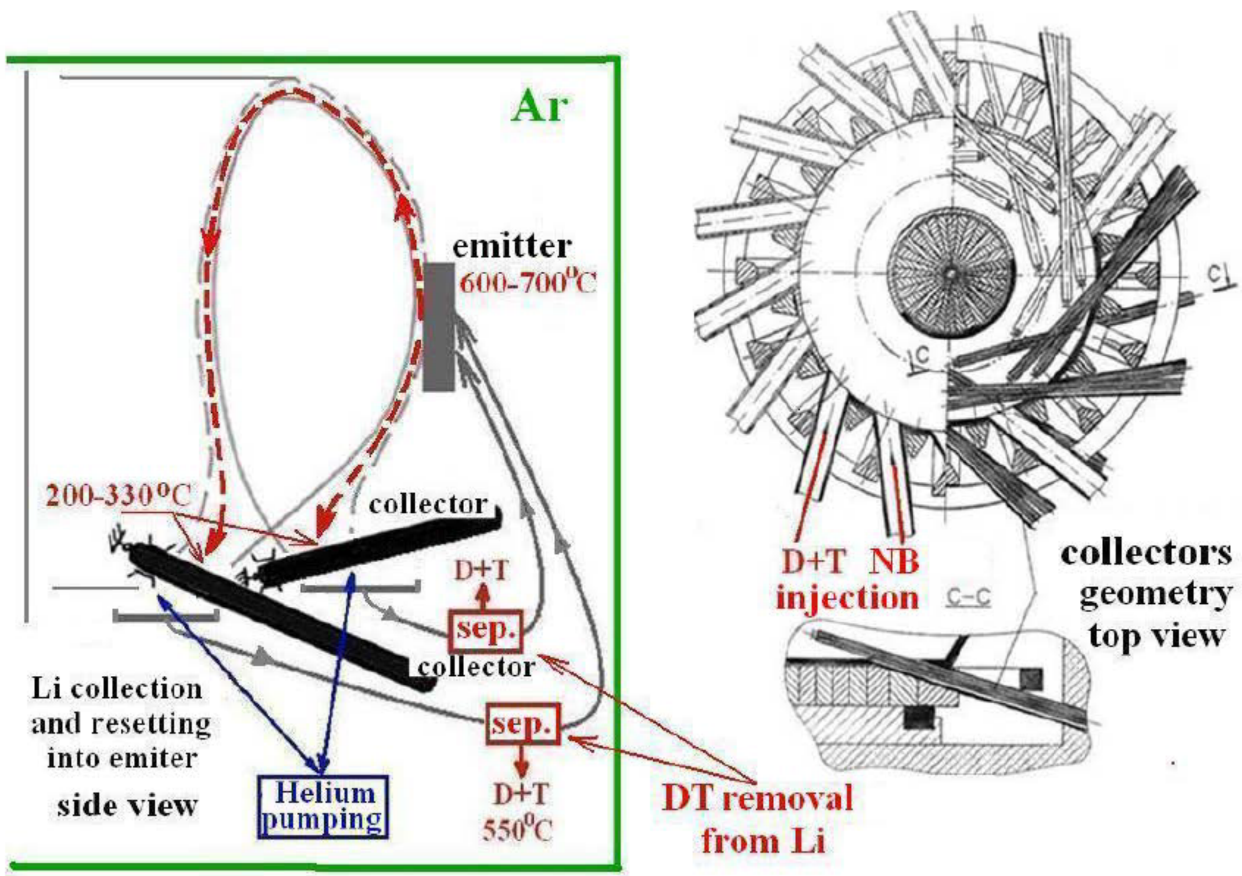

FIG.1. The scheme of a steady-state FNS with lithium emitter–collector circulation.

Active radiative liquid lithium divertor

After Ono et al. FED(2014)in press.

Radiative Liquid Lithium Divertor

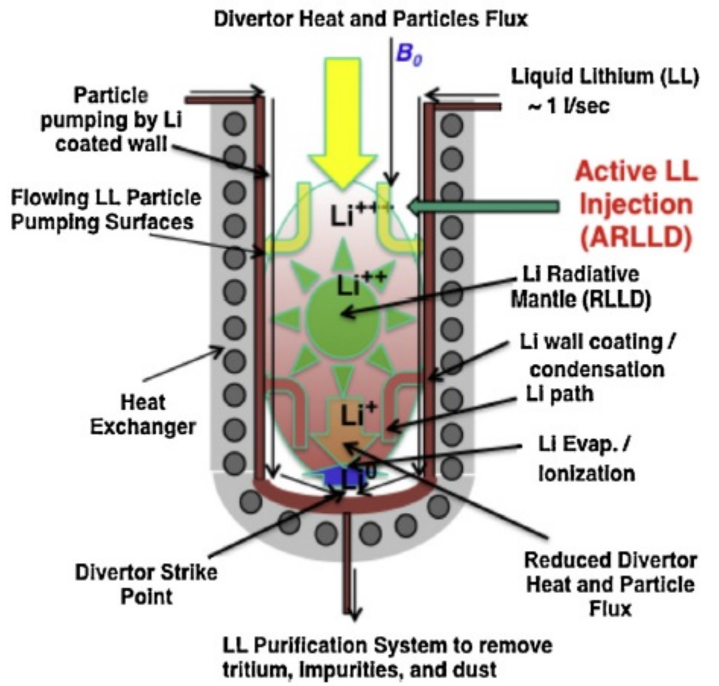

Fig. 2. A simplified schematic of RLLD chamber. The LL flows down along the side wall to provide pumping, and the thicker LL layer at the bottom provides radiative Li source for heat flux reduction and divertor substrate protection. A new feature is the active LL injection from the side wall.

"RLLD" implemented in a reactor

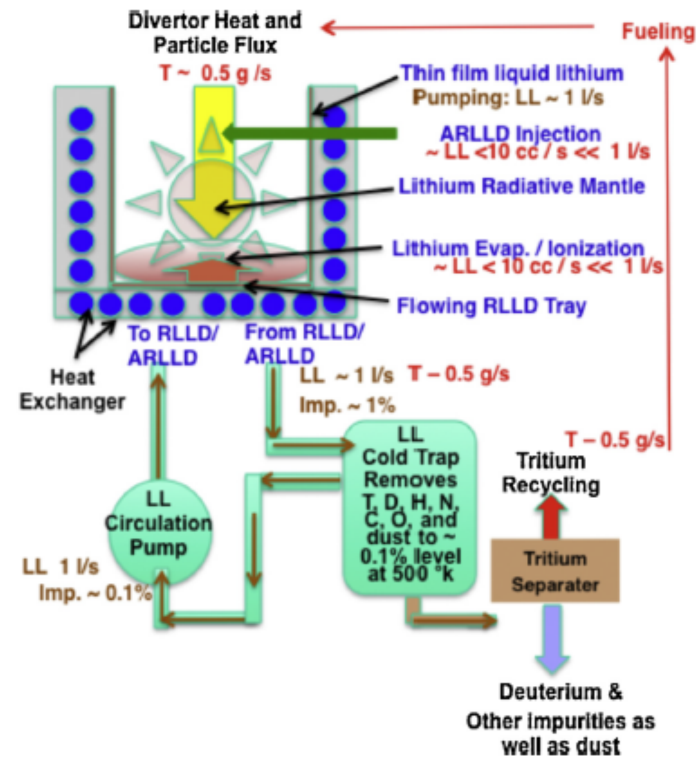

Fig. 9. A schematic for the LL purification loop for ARLLD/RLLD in a power plant.

POP on particle control by Li-gettered MS-PFC

(Presented at ANS-TOFE, 2002)

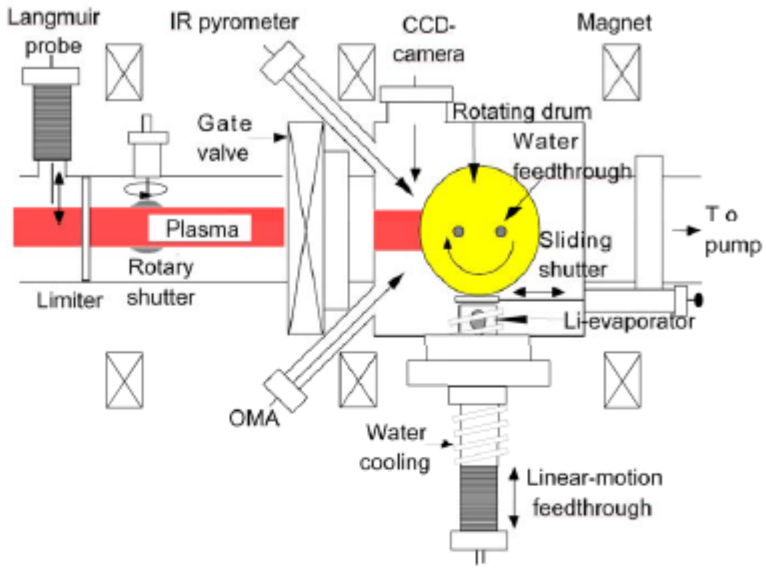

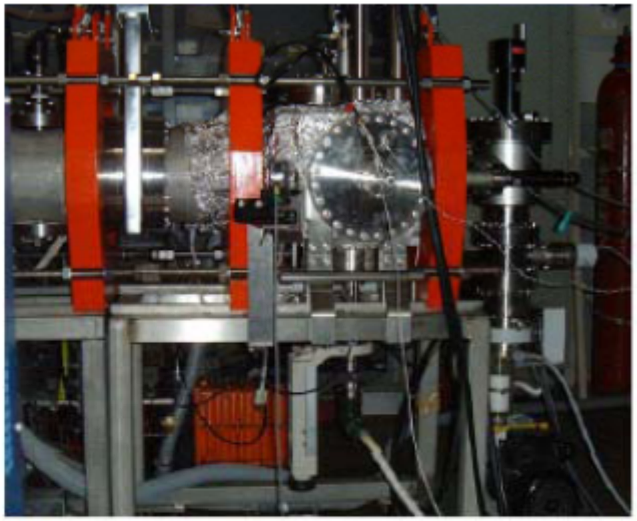

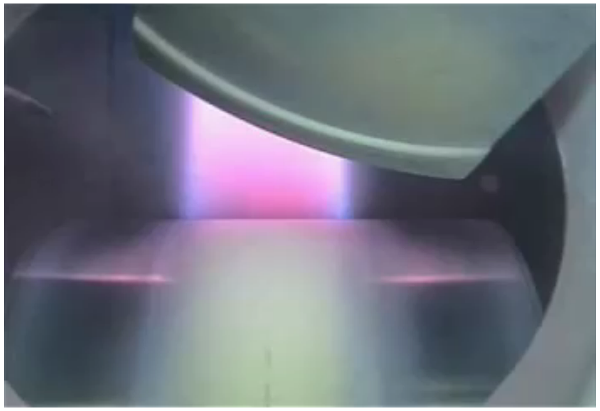

Power/particle handling issues with the Liquid Lithium Divertor

LLD in NSTX

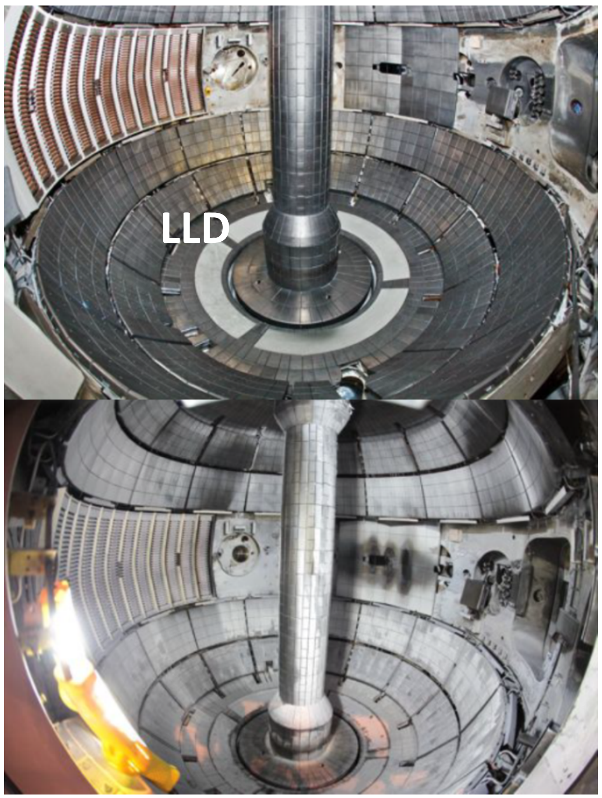

Kugel et al. Fusion Eng. Des. 87(2012)1724

Buoying impurities: LiO2, LiOH

$Li + O_2 \Rightarrow LiO_2$

$H_2 + 1/2O_2 \Rightarrow$ **H_2O**

$Li + H_2O \Rightarrow Li(OH) +$ **$1/2H_2$ => High recycling**

Surface heating->~~Natural convection~~

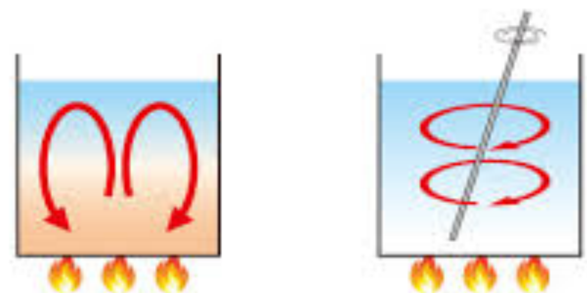

Natural convection

Forced convection

Steady state plasma device at NIFS: VEHICLE-1

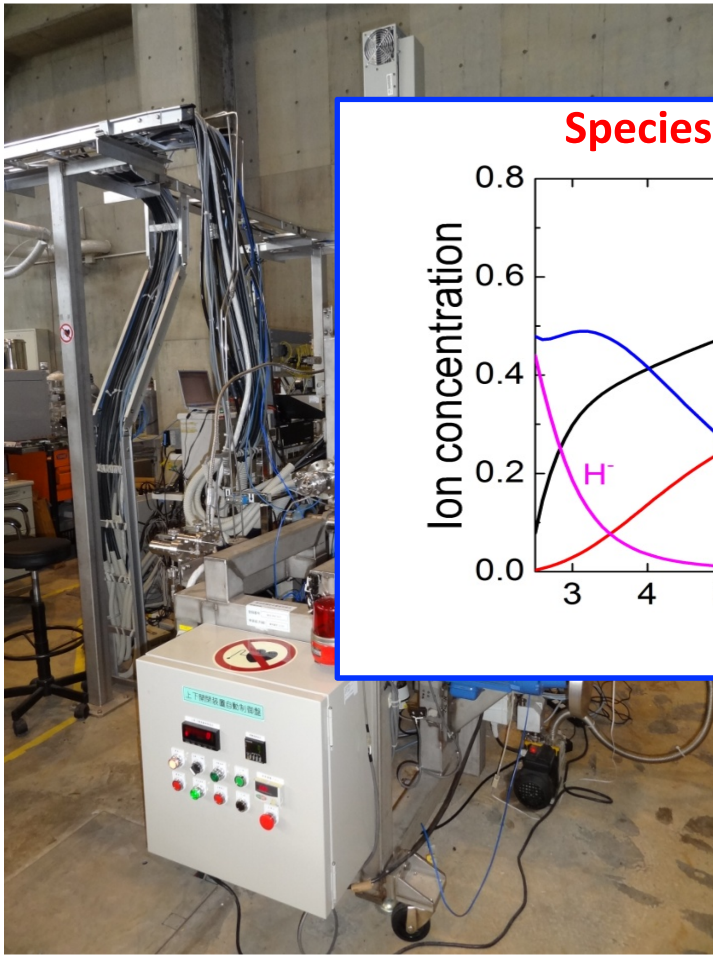

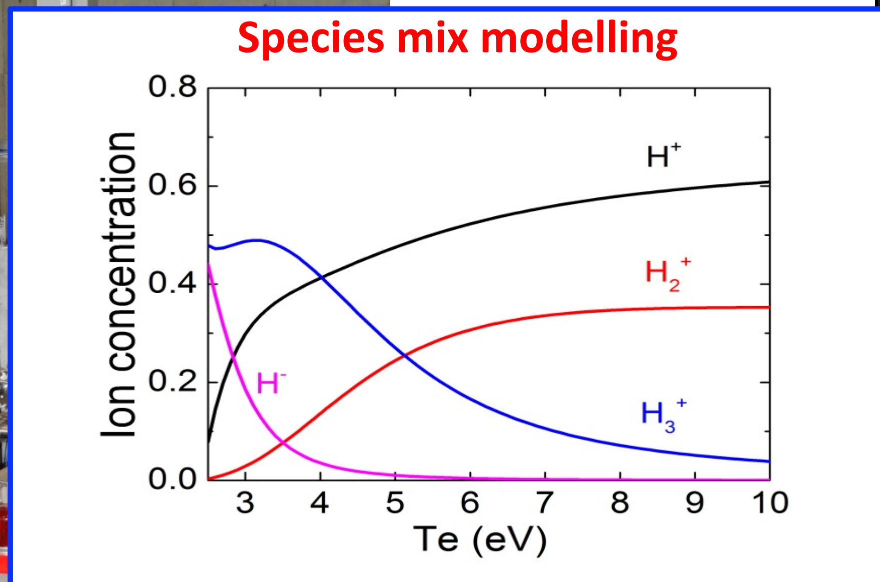

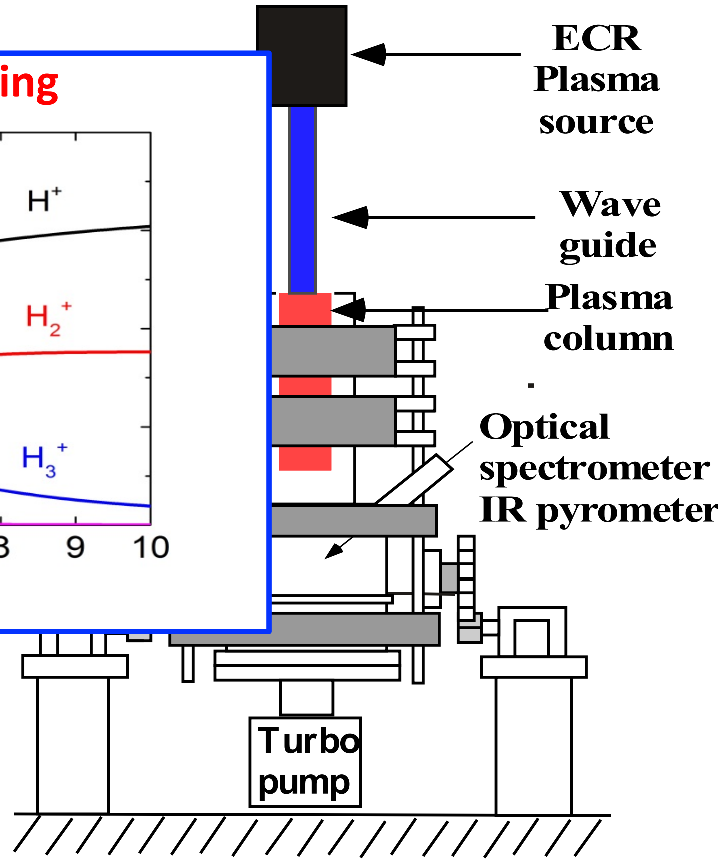

Liquid metal stirring experimental setup

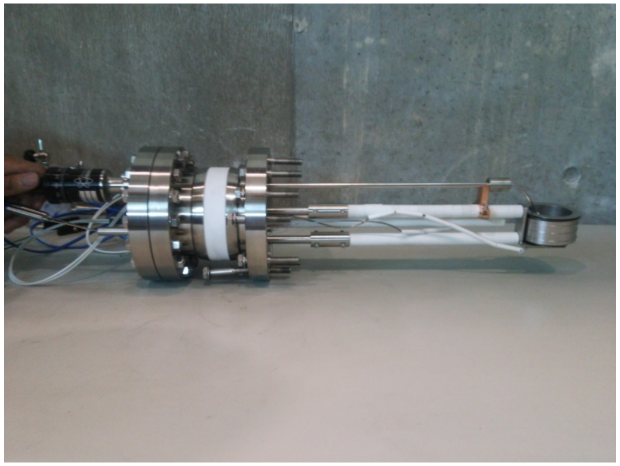

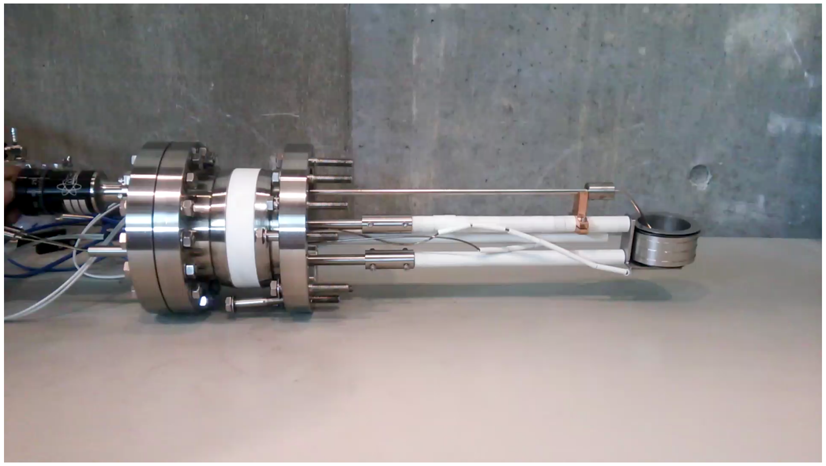

Hydrogen and helium solubility in lithium

Hydrogen solubility in lithium

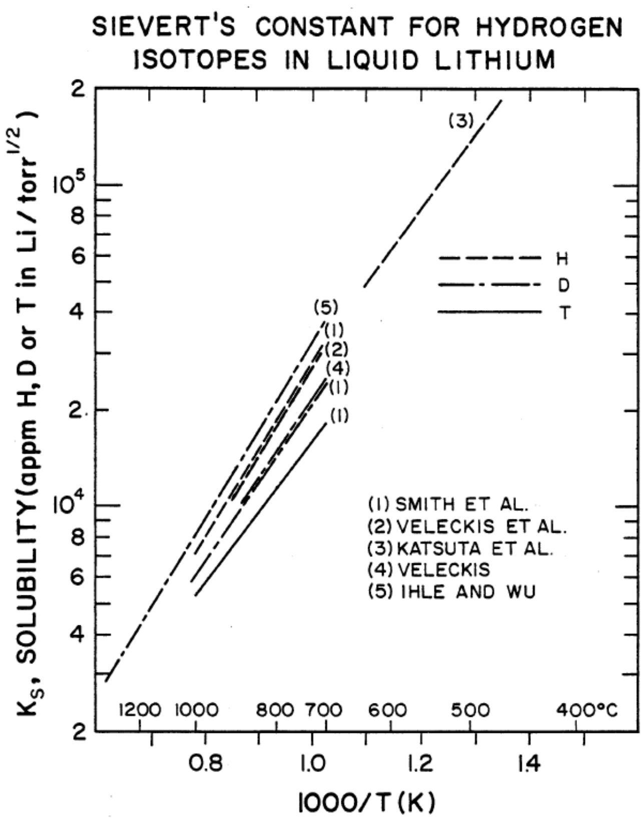

Helium solubility in lithium

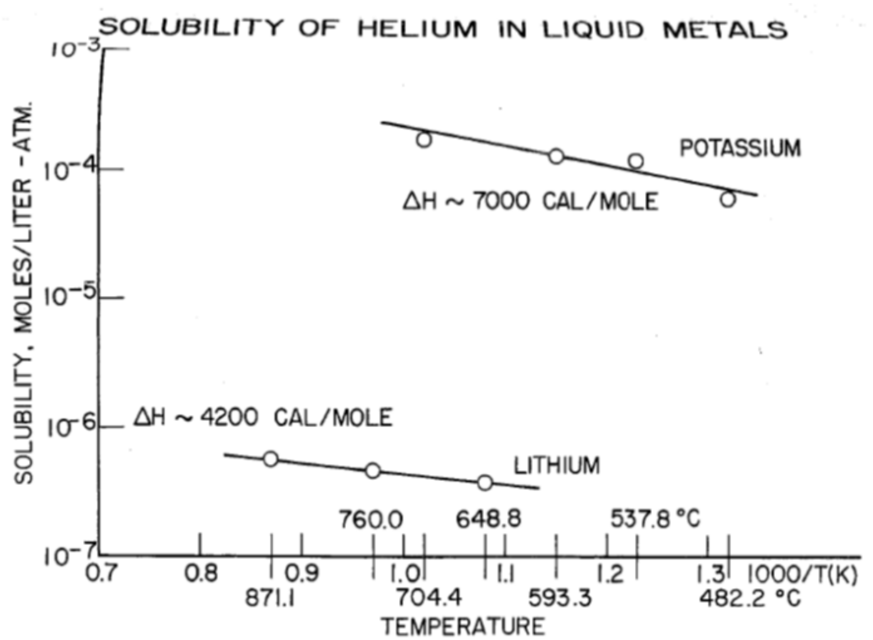

Liquid stirring effects on hydrogen recycling

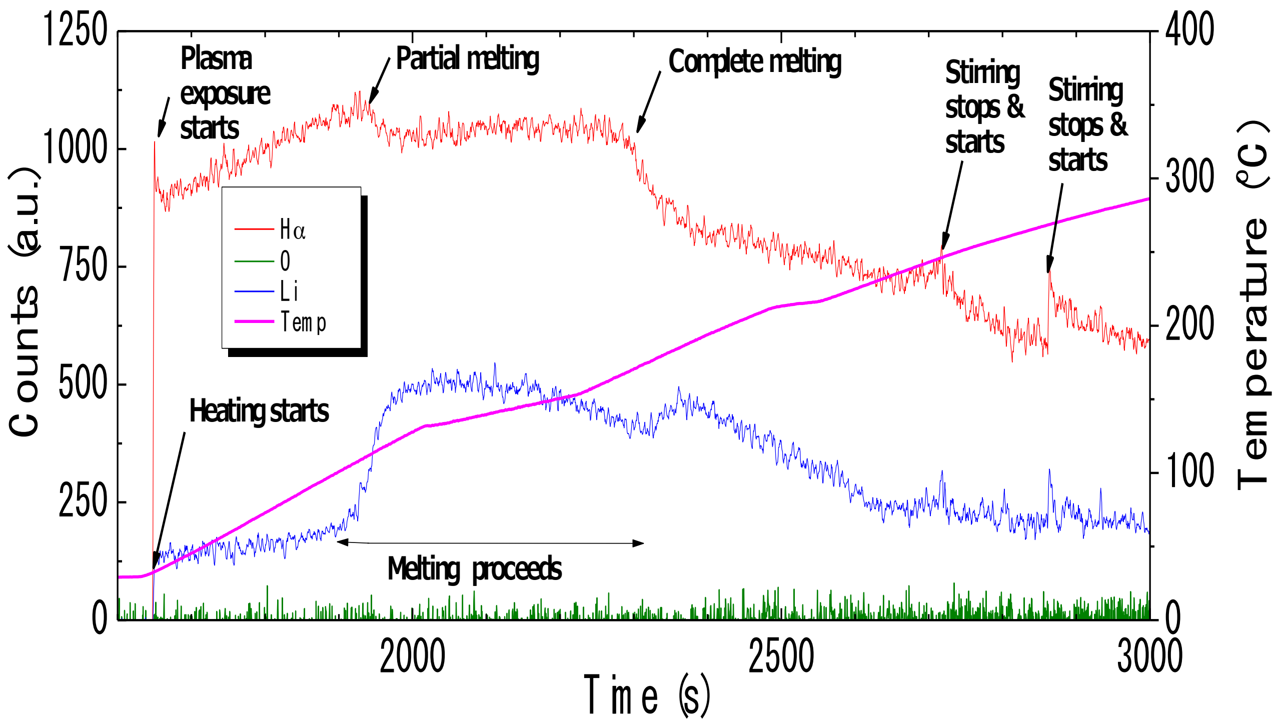

Hirooka et al. Fusion Eng. Des. (2014) in press

Liquid stirring effects on helium recycling

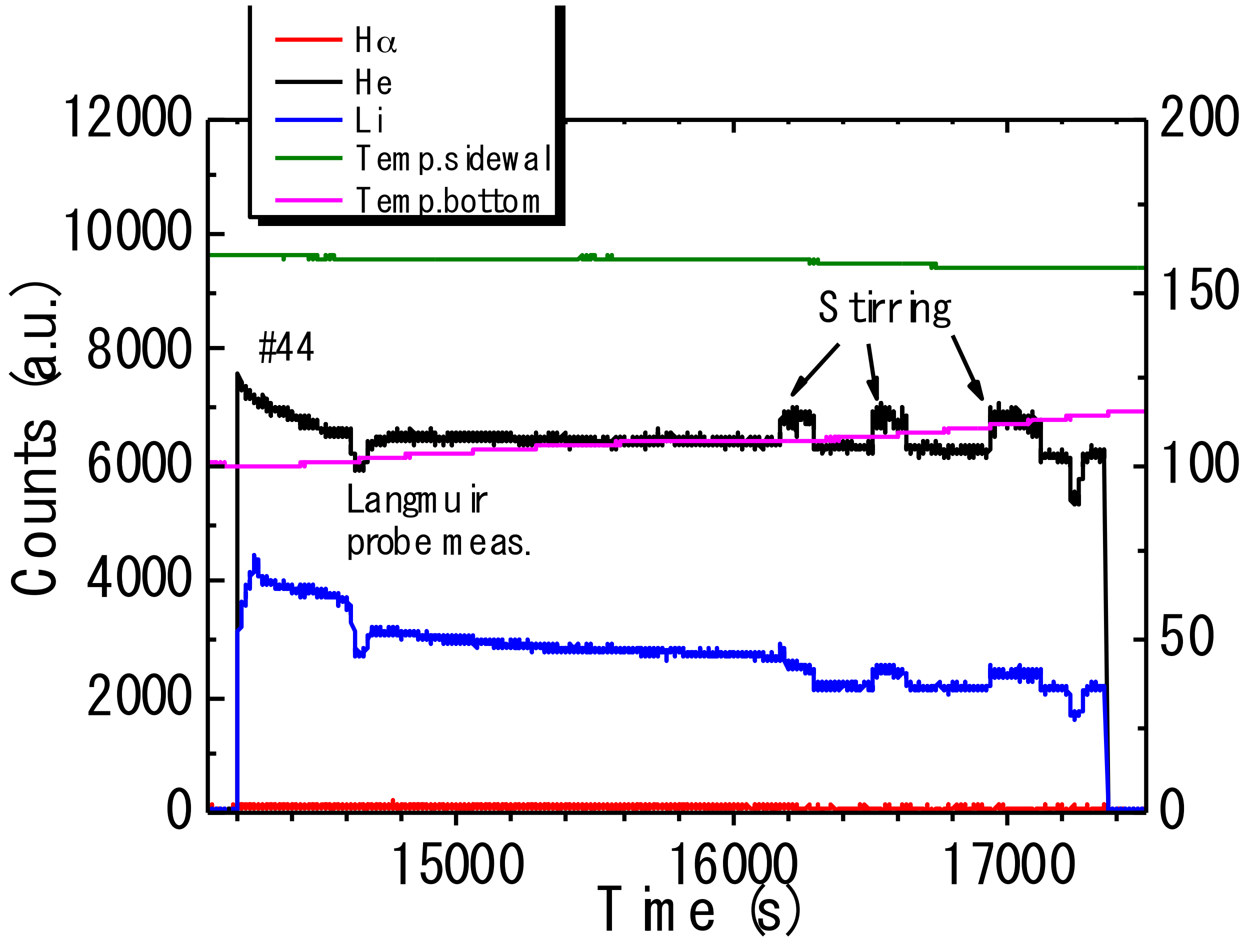

Hirooka et al. Fusion Eng. Des. (2014) in press

TE-MHD: JxB force-driven liquid metal PFC

After Jaworski (PPPL)

PoP experiments in HT-7(@AS-IPP)

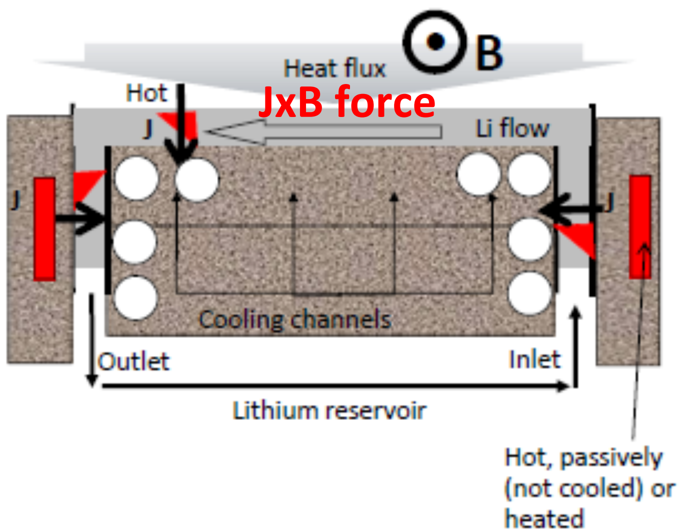

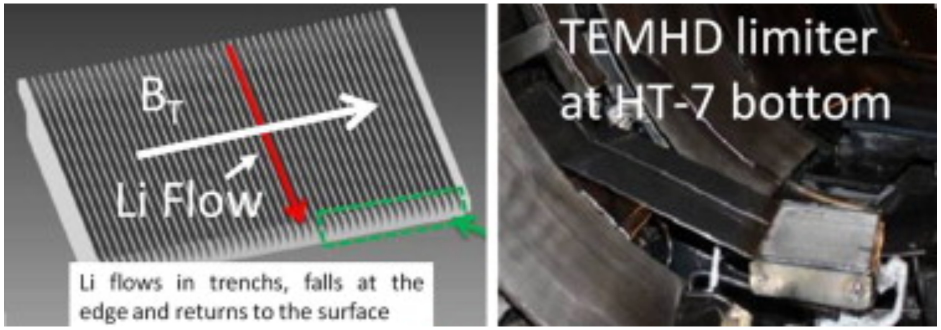

Zuo et al. Fusion Eng. Des. (2014) in press

ACLMD: JxB forced convection liquid metal PFC

After Shimada and Hirooka

PoP experiment at NIFS

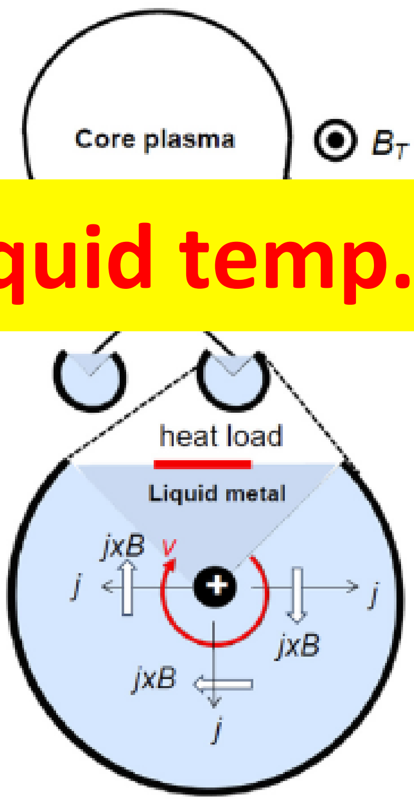

Liquid temp. externally controllable!!

Nucl. Fusion 54 (2014) 122002

Liquid metal: $Ga_{67}\ In_{20.5}\ Sn_{12.5}$

Potential issues with ACLMD

Electro-chemistry effects ↔ Joule heating effects

Standard electrode potential*: E^o

- Li E^o=-3.045V
- Al E^o=-1.67V
- Cr E^o=-0.74V
- Fe E^o=-0.44V
- Ni E^o=-0.24V
- W E^o=-0.58V
- Sn E^o=-0.14V
- H E^o=0.0V
- Ag E^o= +0.79eV
- Au E^o= +1.52eV

* $\Delta G^o = -zFE^o$ (z: # of electrons
F: Faraday's const.)

JxB force heating power: J･V

In the case of our PoP exps. on ACLMD:

- J~20[A]
- V~2.9[V] when rotation starts at 6 rpm
- P~60[W]

The temperature of $Ga_{67}\ In_{20.5}\ Sn_{12.5}$ alloy (320cc) was felt about 50^{o}C. After a while, however, the rotation stops, which indicates a temperature effect on electrochemical properties of (liquid) metals.

Summary and technical implications

1. Present status of liquid metals and/or their vapor/deposits to be used as PFCs has been reviewed with the emphasis on power and particle handling requirements.
2. Implications are: liquid metals needs to be flowing with forced convection for better temperature control and hydrogen absorptivity.
3. Several Innovative concepts to overcome the MHD drag have been proposed, showing successful PoP. However, there is a long way to go to reach the same level of technical maturity as the present-day divertor concept. We must count on the next generation scientists!